Electronic Supplementary Material (ESI) for Dalton Transactions.

Hexagonal $Sr_{1-x/2}Al_{2-x}Si_xO_4:Eu^{2+},Dy^{3+}$ transparent ceramics exhibiting white persistent luminescence excitable by visible light.

Victor Castaing*[a], Charlotte Monteiro[b], Atul D. Sontakke[a, c], Kazuki Asami[d], Jian Xu[d], Alberto J. Fernández Carrión[b, e], Mikhail G. Brik[f], Setsuhisa Tanabe[d], Mathieu Allix[b] and Bruno Viana*[a].

a. Chimie ParisTech, PSL University, CNRS, Institut de Recherche de Chimie Paris, 11 rue Pierre et Marie Curie, 75005 Paris, France.

b. CNRS, CEMHTI UPR3079, Université Orléans, F-45071 Orléans, France.

c. Condensed Matter & Interfaces, Debye Institute for Nanomaterials Science, Utrecht University, Princetonplein 1, 3584 CC Utrecht, The Netherlands.

d. Graduate School of Human and Environmental Studies, Kyoto University, Kyoto 606-8501, Japan.

e. MOE Key Laboratory of New Processing Technology for Nonferrous Metals and Materials, Guangxi Universities Key Laboratory of Non-ferrous Metal Oxide Electronic Functional Materials and Devices, College of Materials Science and Engineering, Guilin University of Technology, Guilin 541004, P. R. China.

f. Institute of Physics, University of Tartu, W. Ostwald Str. 1, Tartu, 50411, Estonia.

KEYWORDS: $SrAl_2O_4$-based transparent ceramics, persistent color tuning, w-LED charging, persistent luminescence mechanism.

Supporting Information:

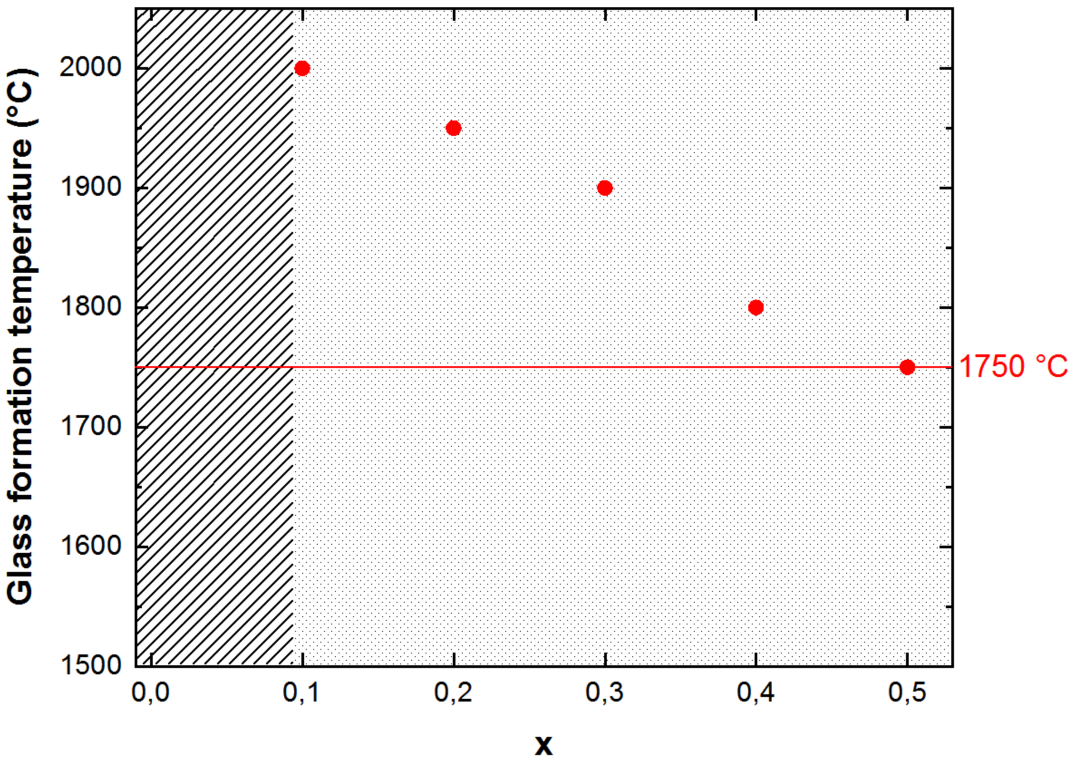

Fig. S1: Temperature used for glass precursor elaboration as a function of the material composition. For compositions with x ≤ 0.1, no glass can be obtained from the melt. For x ≥ 0.1 the glass formation temperature decreases with the Si content increase.

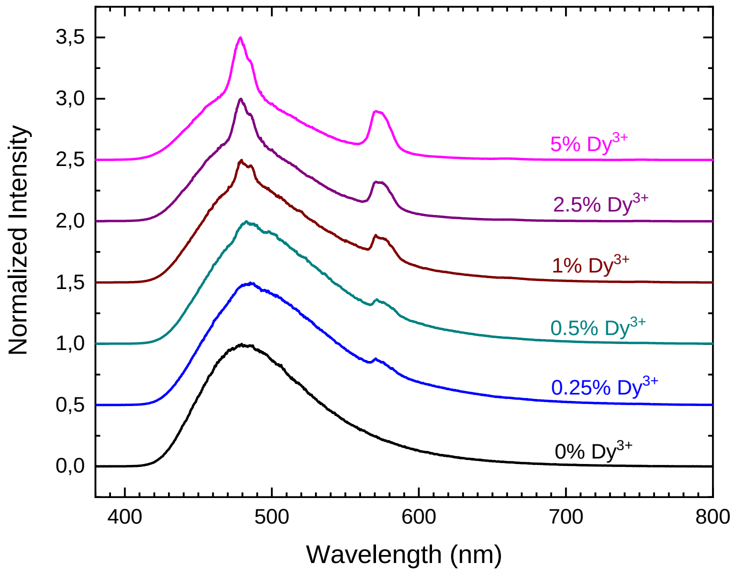

Fig. S2: PL spectra of $Sr_{0.75}Al_{1.5}Si_{0.5}O_4$:$Eu^{2+}$,$Dy^{3+}$. The Dy^{3+} content was varied from 0 % to 5 % relatively to Sr.

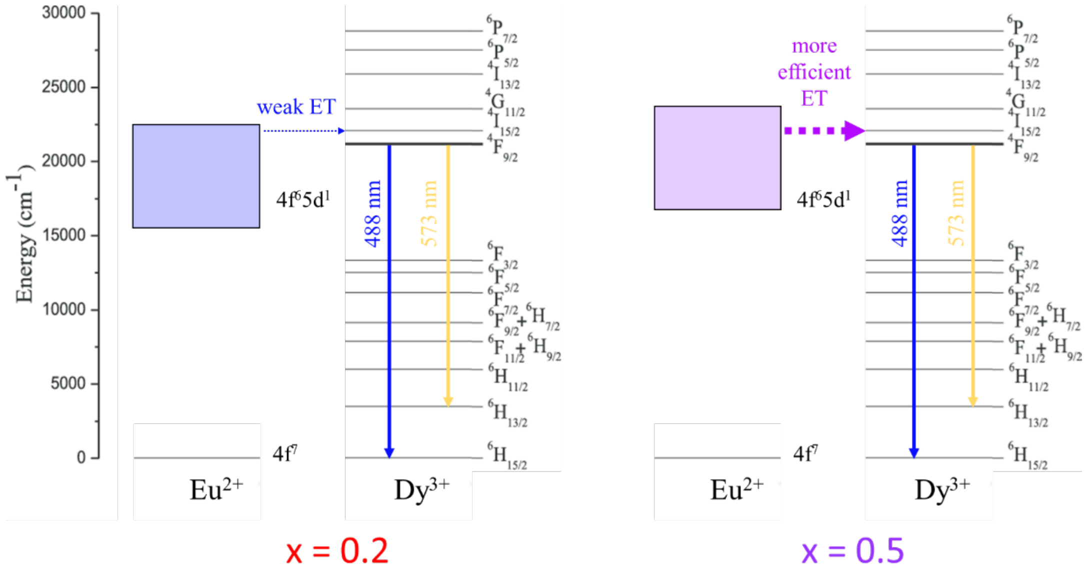

Fig. S3: Schematized energy level diagrams of Eu^{2+} and Dy^{2+} in h-SASO 0.2 (left) and 0.5 (right).

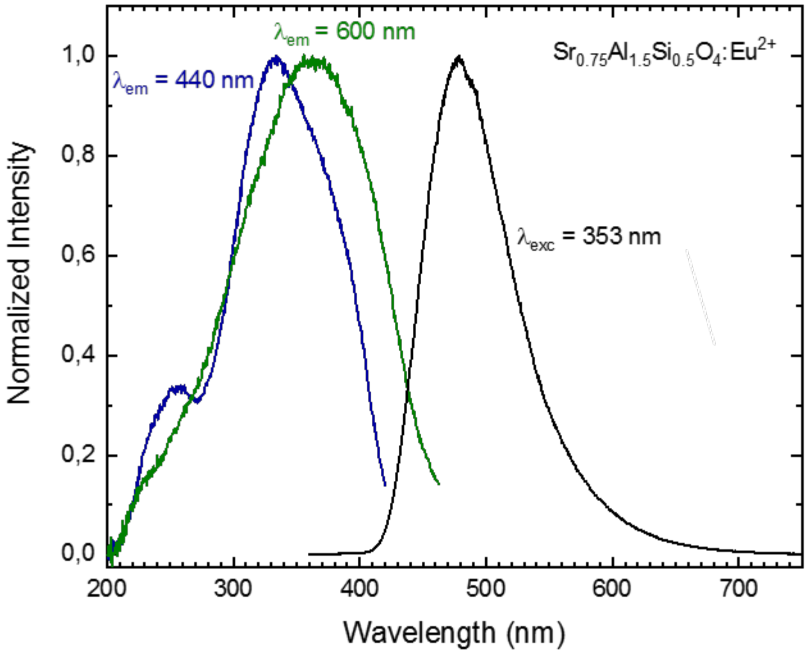

Fig. S4: (black) PL spectrum of $Sr_{0.75}Al_{1.5}Si_{0.5}O_4$:$Eu^{2+}$ with λ_{exc} = 353 nm and comparison of PLE spectra for different emission wavelength: (blue) λ_{em} = 440 nm and (green) λ_{em} = 600 nm.

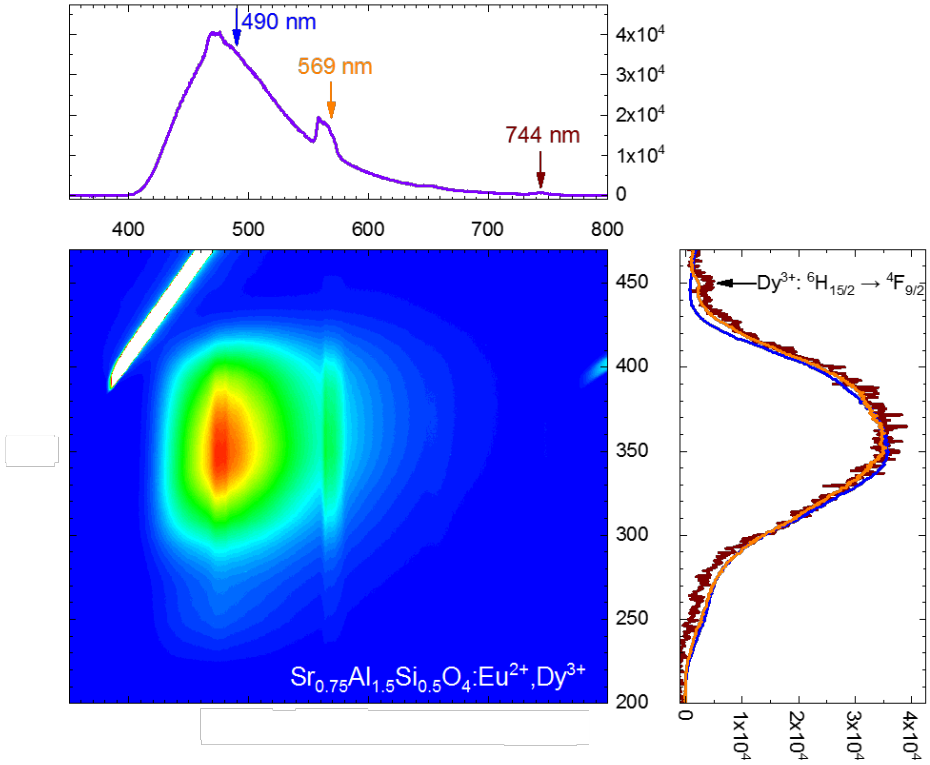

Fig. S5: PL/PLE plot of SASO x = 0.5 sample. The upper emission spectra is recorded for λ_{exc} = 350 nm. The side excitation spectra are recorded for pure Eu^{2+} emission, Eu^{2+} mixed overlapped Dy^{3+} emission and pure Dy^{3+} emission (λ_{em} = 490, 569 and 744 nm respectively). The intensity of the excitation spectra for 569 nm and 744 nm emissions have been multiplied by 2.3 and 48 respectively in order to be comparable with the pure Eu^{3+} one.

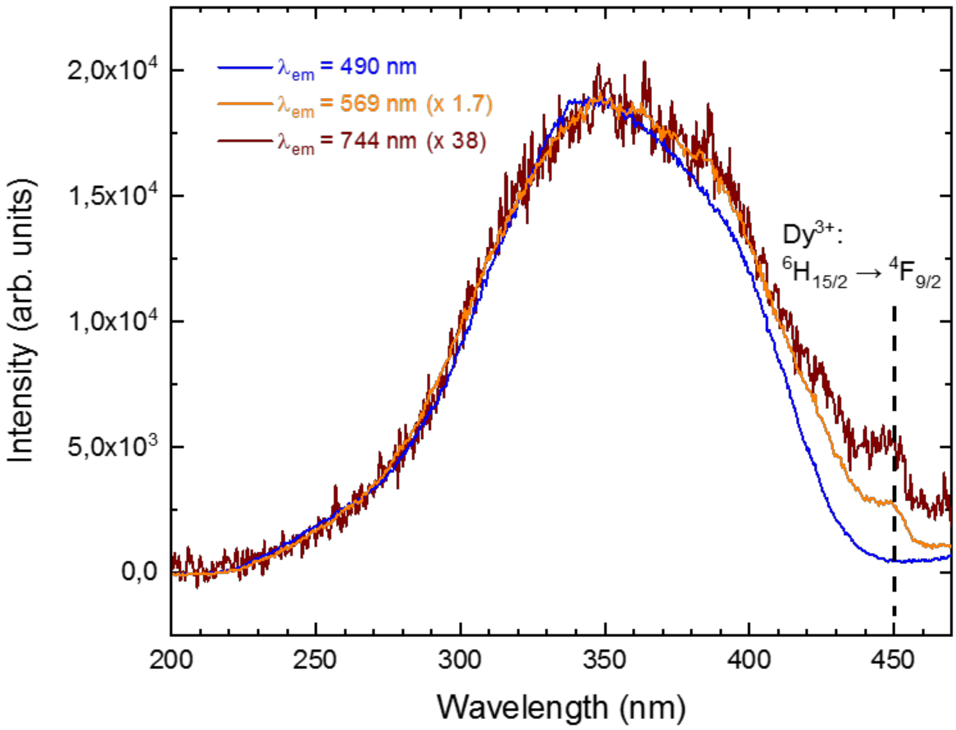

Fig. S6: Comparison of SASO x = 0.5 with 5 % Dy^{3+} doping concentration PLE spectra recorded at different wavelengths, λ_{em} = 490, 569 and 744 nm (blue, orange and dark red plots respectively).

Supporting Information S7: Eu^{2+} red shift evolution with the materials composition.

The europium excitation redshift in a compound $Sr_{1-x/2}Al_{2-x}Si_xO_4$, $D(Eu^{2+}, Sr_{1-x/2}Al_{2-x}Si_xO_4)$ is expected to be the result of (i) the crystal field splitting $\varepsilon_{cfs}(Eu^{2+}, Sr_{1-x/2}Al_{2-x}Si_xO_4)$ and (ii) the centroid shift $\varepsilon_c(Eu^{2+}, Sr_{1-x/2}Al_{2-x}Si_xO_4)$ as described in the following equation:

$$D\left(Eu^{2+}, Sr_{1-\frac{x}{2}}Al_{2-x}Si_xO_4\right) = \varepsilon_c\left(Eu^{2+}, Sr_{1-\frac{x}{2}}Al_{2-x}Si_xO_4\right) - \Delta\varepsilon_c(Eu^{2+}, free) + \frac{\varepsilon_{cfs}\left(Eu^{2+}, Sr_{1-\frac{x}{2}}Al_{2-x}Si_xO_4\right)}{r\left(Eu^{2+}, Sr_{1-\frac{x}{2}}Al_{2-x}Si_xO_4\right)} + \Delta\varepsilon_{cfs}(Eu^{2+}, free) \quad \text{(eq1)}$$

Using semi-empirical formula, it is possible to relate the crystal field splitting and the centroid shift to the size and nature of the coordination polyhedral.

$$\varepsilon_{cfs} = \frac{\beta_{poly}^{Q}}{d_{av}^{2}} \quad \text{(eq2)}$$

$$\frac{\varepsilon_c}{CN} = \frac{\alpha_{sp} e^2}{4\pi\varepsilon_0 d_{eff}^6}\left(\langle\psi_{5d}|r^2|\psi_{5d}\rangle - \langle\psi_{4f}|r^2|\psi_{4f}\rangle\right) \quad \text{(eq3)}$$

In these expressions, β is a constant parameter describing the type of the coordination polyhedral, assumed to be constant along the solid solution. α_{sp} represents the spectroscopic polarizability, related to the average cation electronegativity as follows:

$$\alpha_{sp} \equiv \frac{1}{\chi_{av}^2} \quad \text{(eq4)}$$

with

$$\chi_{av} \equiv \frac{1}{N_a}\sum_{i}^{Nc}\frac{z_i\chi_i}{\gamma} \quad \text{(eq5)}$$

The evolution of the average and effective Eu-O bond distances calculated using eq6 and eq7 are reported in the figure S8 for x = 0.2, 0.3 and 0.5 using the synchrotron experimental data.

$$\frac{1}{d_{eff}^6} = \frac{1}{CN}\sum_{i=1}^{CN}\frac{1}{\left[d_i - f\left(R_{Sr^{2+}} - R_{Eu^{2+}}\right)\right]^6} \quad \text{(eq6)}$$

$$d_{av} = \langle d\rangle - f\left(R_{Sr^{2+}} - R_{Eu^{2+}}\right) \quad \text{(eq7)}$$

With f = 0.6, $R_{Sr^{2+}} = 1.32\ \text{Å}\ and\ R_{Eu^{2+}} = 1.31\ \text{Å}$. In this figure, the warning signs remind to be aware that the Sr_4 and Sr_5 sites are linearly emptied along the solid solution.

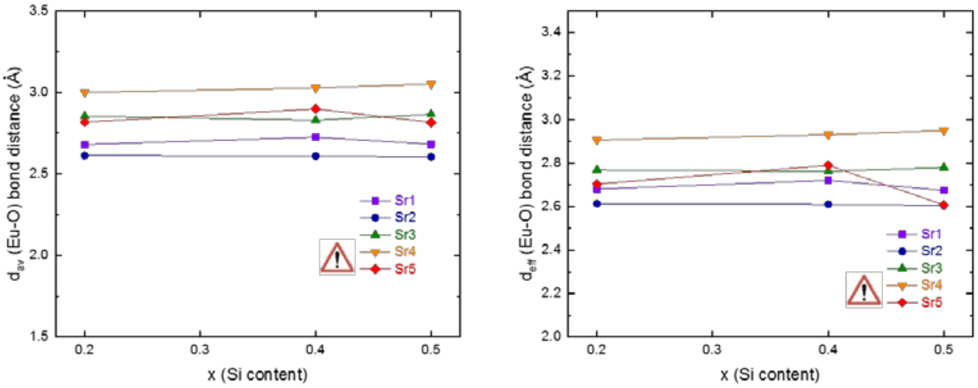

Fig. S8: Evolution of the Eu-O bond distances for the five distinct Sr sites along the solid solution. On the left, the Eu-O average bond distances are presented whereas the effective bond distances are displayed on the right. The warning signs remind that Sr_4 and Sr_5 sites are partially emptied along the solid solution.

Assuming that Eu^{2+} can occupy each Sr^{2+} site (not vacancy), no clear average and effective Eu-O bond distances can be depicted, in contrast with the clear Eu^{2+} blue shift observed. On the other hand, the counter cation electronegativity changes from $\chi_{Al} = 1.47$ to $\chi_{Si} = 1.74$. Using eq. X, it is observable that χ_{av} increases along the solid solution, leading to a decrease of the optical polarizability as indicated in Figure S9. This decrease of the optical polarizability, which results in a decrease of the centroid shift, may be an explanation of the blue shift observed along the solid solution.

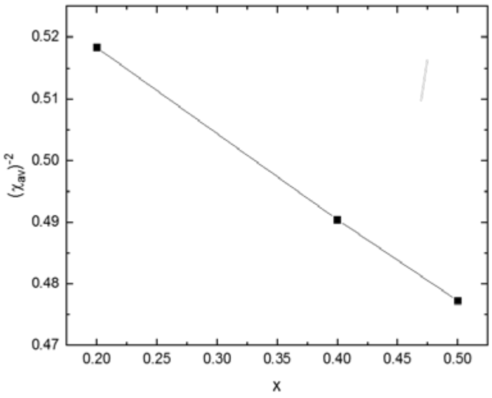

Fig. S9: Evolution of the spectroscopic polarizability in the h-SASO x materials (0.2 ≤ x ≤0.5).

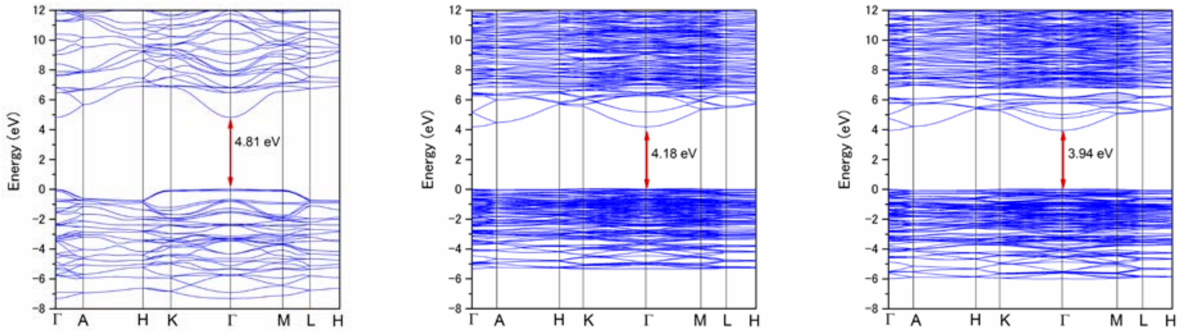

Fig. S10: Band structures of $Sr_{1-x/2}Al_{2-x}Si_xO_4$ x = 0(left), x = 0.2 (middle) and x = 0.5 (right)

The density functional theory (DFT) calculations of the structural and electronic properties of $Sr_{1-x/2}Al_{2-x}Si_xO_4$ (x =0, 0.2 and 0.5) were performed using the CASTEP module of Materials Studio 2017[1] package and the GGA-PBE functionals[2]. The ionic core electrons were replaced by on-the-fly ultrasoft pseudopotentials implemented in the CASTEP with the following electronic configuations: [Kr] $4s^2$ $4p^6$ $5s^2$ for Sr, [Ne] $3s^2$ $3p^1$ for Al, [Ne] $3s^2$ $3p^2$ for Si and [He] $2s^2$ $2p^4$ for O [3]. Relativistic effects were taken into account at the level of the Koelling-Harmon approximation of the Dirac equation [4]. The plane-wave basis energy cut-off was chosen as 630.0 eV and *k*-point grids were chosen as 3×2×2 for x = 0 and 2×2×2 for x = 0.2 and 0.5. The convergence parameters were as follows: total energy tolerance 5.0×10^{-6} eV/atom, maximum force tolerance 0.01 eV/Å, maximum stress component 0.02 GPa and maximum displacement 5.0×10^{-4} Å.

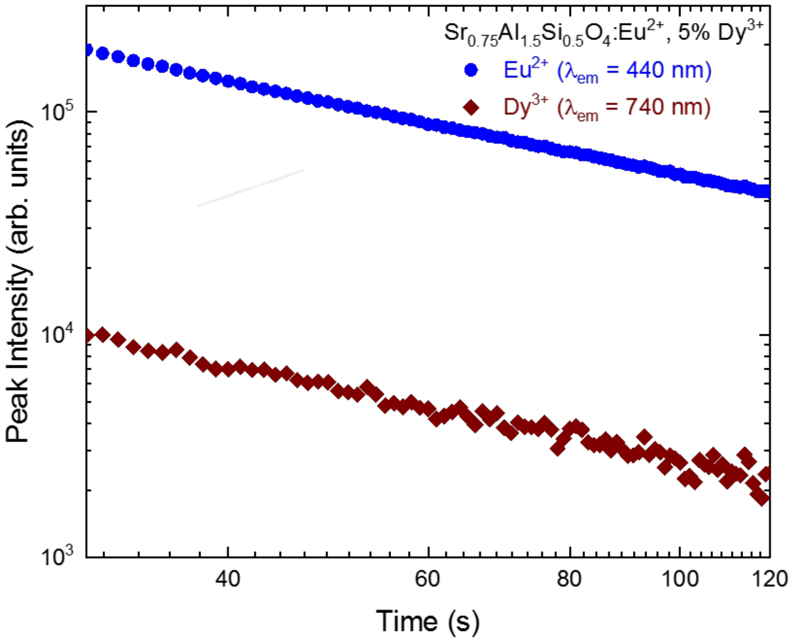

Fig. S11: Comparison of Eu^{2+} and Dy^{3+} persistent decays in the sample h-$Sr_{0.75}Al_{1.5}Si_{0.5}O_4$ with a 5 % Dy^{3+} doping concentration after 365 nm excitation for 5 min at RT.

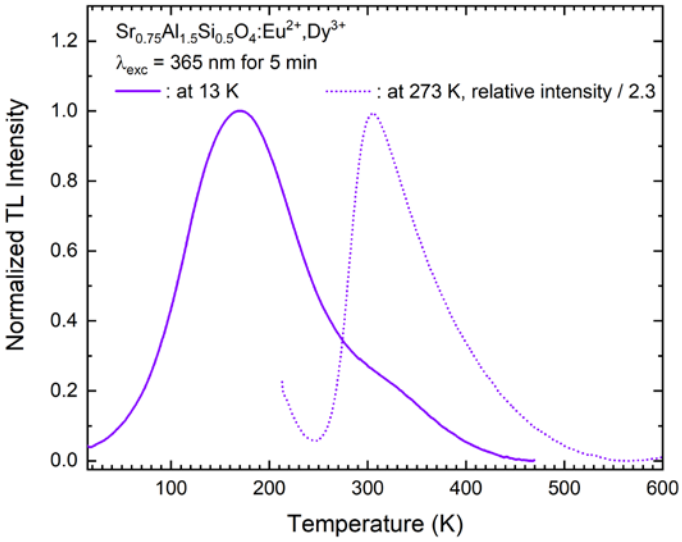

Fig. S12: Comparison of Eu^{2+} and Dy^{3+} persistent decays in the sample h-$Sr_{0.75}Al_{1.5}Si_{0.5}O_4$ with a 5 % Dy^{3+} doping concentration after 365 nm excitation for 5 min at RT. Note that in order to normalize, the intensity of the TL glow curve with excitation at 273 K has been divided 2.3 times more than the low temperature one.

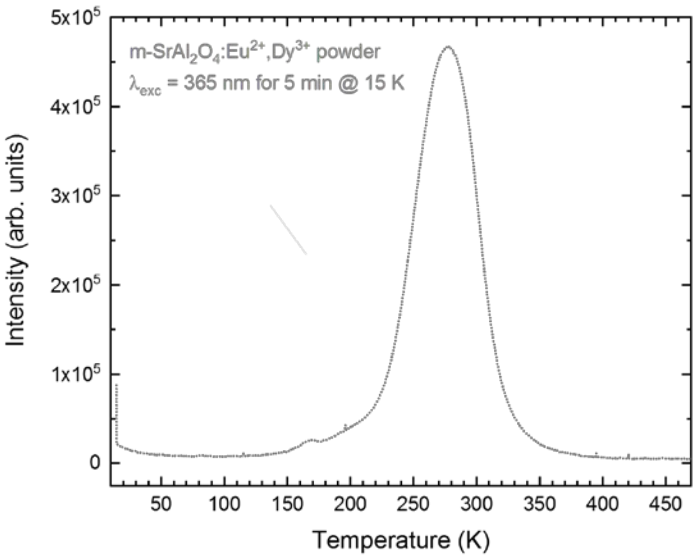

Fig. S13: Thermoluminescence glow curve of the monoclinic $SrAl_2O_4:Eu^{2+},Dy^{3+}$ powder obtained by the ADL method. Prior to recording, the material have been excited using the 365 nm LED for 5min at 15 K.

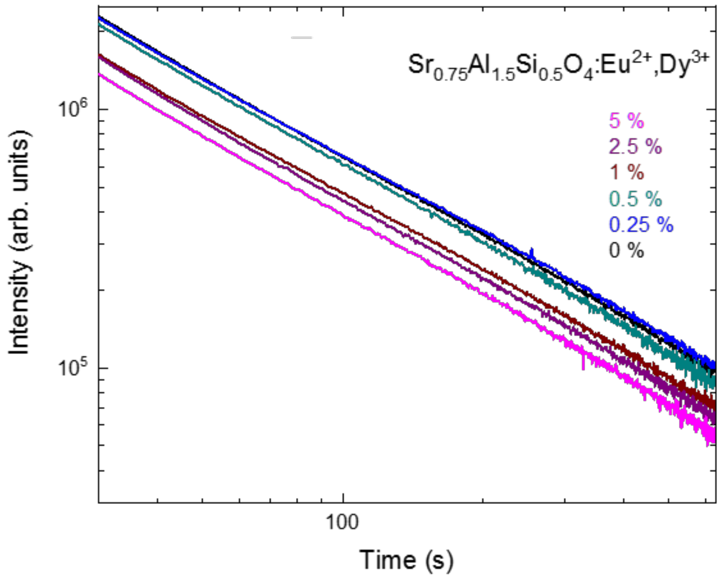

Fig. S14: Persistent luminescence decay curves of $Sr_{0.75}Al_{1.5}Si_{0.5}O_4:Eu^{2+},Dy^{3+}$ with Dy^{3+} contents ranging from 0 % to 5%.

References

(1) S.J. Clark, M.D. Segall, C.J. Pickard, P.J. Hasnip, M.J. Probert, K. Refson, M.C. Payne, Zeitschrift Für Krist. 220 (2005) 567–570.

(2) J.P. Perdew, K. Burke, M. Ernzerhof, Phys. Rev. Lett. 77 (1996) 3865.

(3) D. Vanderbilt, Phys. Rev. B. 41 (1990) 7892–7895.

(4) D.D. Koelling, B.N. Harmon, J. Phys. C. 10 (1977) 3107.